Testing fluvial erosion models using the transient response of bedrock rivers to tectonic forcing in the Apennines, Italy

M. Attal,[1] P. A. Cowie,[1] A. C. Whittaker,[2] D. Hobley,[1] G. E. Tucker,[3] and G. P. Roberts[4]

Received 6 September 2010; revised 15 January 2011; accepted 4 February 2011; published 16 April 2011.

[1] The transient response of bedrock rivers to a drop in base level can be used to discriminate between competing fluvial erosion models. However, some recent studies of bedrock erosion conclude that transient river long profiles can be approximately characterized by a transport-limited erosion model, while other authors suggest that a detachment-limited model best explains their field data. The difference is thought to be due to the relative volume of sediment being fluxed through the fluvial system. Using a pragmatic approach, we address this debate by testing the ability of end-member fluvial erosion models to reproduce the well-documented evolution of three catchments in the central Apennines (Italy) which have been perturbed to various extents by an independently constrained increase in relative uplift rate. The transport-limited model is unable to account for the catchments' response to the increase in uplift rate, consistent with the observed low rates of sediment supply to the channels. Instead, a detachment-limited model with a threshold corresponding to the field-derived median grain size of the sediment plus a slope-dependent channel width satisfactorily reproduces the overall convex long profiles along the studied rivers. Importantly, we find that the prefactor in the hydraulic scaling relationship is uplift dependent, leading to landscapes responding faster the higher the uplift rate, consistent with field observations. We conclude that a slope-dependent channel width and an entrainment/erosion threshold are necessary ingredients when modeling landscape evolution or mapping the distribution of fluvial erosion rates in areas where the rate of sediment supply to channels is low.

Citation: Attal, M., P. A. Cowie, A. C. Whittaker, D. Hobley, G. E. Tucker, and G. P. Roberts (2011), Testing fluvial erosion models using the transient response of bedrock rivers to tectonic forcing in the Apennines, Italy, *J. Geophys. Res.*, *116*, F02005, doi:10.1029/2010JF001875.

1. Introduction

[2] Rivers incising into bedrock lower the base level for hillslope erosion processes. They communicate changes in external forcing (tectonics, climate) to the hillslopes and thus drive the evolution of nonglaciated mountainous landscapes. Among the models of fluvial incision which have been proposed over the last decades, the "detachment-limited" and "transport-limited" end-member models have been popular within the geomorphology community, thanks to their simple formulation which makes them easy to parameterize and to implement into numerical models of landscape evolution. Detachment-limited models in particular assume in their simplest form that fluvial incision is proportional to specific stream power (SSP) or shear stress, which depend on river discharge and channel geometry, and that sediment is evacuated without influencing river dynamics (in the following, we will refer to these models as "linear SSP" and "linear shear stress" models, respectively) [e.g., *Howard and Kerby*, 1983; *Seidl and Dietrich*, 1992]. Detachment-limited models were given support by several studies which showed that the dynamics of bedrock rivers in various tectonic and climatic contexts could be explained by the detachment-limited model [e.g., *Stock and Montgomery*, 1999; *Whipple et al.*, 2000a; *Kirby and Whipple*, 2001], subsequently modified by the introduction of a threshold for erosion to account for an observed nonlinear relationship between SSP and relative uplift rate [e.g., *Lavé and Avouac*, 2001; *Snyder et al.*, 2003a, 2003b; *DiBiase et al.*, 2010]. Conversely, the transport-limited model stipulates that fluvial incision is limited by the rate at which sediment particles can be transported away: in a transport-limited system, sediment is always available and the river is always at capacity [e.g., *Willgoose et al.*, 1991; *Tucker and Whipple*, 2002]. Recent studies have showed that in some cases, the transport-limited model may also describe the behavior of rivers incising into

[1]School of GeoSciences, University of Edinburgh, Edinburgh, UK.
[2]Royal School of Mines, Imperial College London, London, UK.
[3]Cooperative Institute for Research in Environmental Sciences and Department of Geological Sciences, University of Colorado at Boulder, Boulder, Colorado, USA.
[4]Research School of Geological and Geophysical Sciences, Birkbeck, University of London, and University College London, London, UK.

0148-0227/11/2010JF001875

bedrock [*Loget et al.*, 2006; *Cowie et al.*, 2008; *Valla et al.*, 2010].

[3] Identifying which of these models best describes the evolution of a fluvial system is important for understanding and modeling geomorphic processes and rates, since different models will predict contrasted landscape responses to a perturbation [e.g., *Tucker and Whipple*, 2002]. It is also essential for extracting tectonic information from river long profiles [e.g., *Kirby and Whipple*, 2001; *Kirby et al.*, 2003; *Wobus et al.*, 2006a], as different models will make different predictions of how channel slope relates to spatial and temporal variations in relative rock uplift rate. *Tucker and Whipple* [2002] showed theoretically that the transient response of a landscape provides potentially the best means to discriminate between and test the different fluvial incision models. Early attempts at objectively testing and calibrating the different models using statistical methods produced mixed results, either due to lack of transient features [*Tomkin et al.*, 2003] or lack of temporal constraints on the transient evolution [*van der Beek and Bishop*, 2003]. More recent studies of the transient response of real bedrock rivers have led to apparently contradictory results, that is, that in some cases the response may be approximated by a transported-limited model [*Loget et al.*, 2006; *Cowie et al.*, 2008; *Valla et al.*, 2010] while in other cases the detachment-limited model approximately describes the response documented in the field [*Whittaker et al.*, 2008; *Attal et al.*, 2008; *Boulton and Whittaker*, 2009].

[4] In this debate over which fluvial incision model should be used to model landscape evolution, the sediment issue is central [*Cowie et al.*, 2008; *Johnson et al.*, 2009; *Valla et al.*, 2010]. In addition to the detachment-limited and transport-limited models, many sediment-flux-dependent fluvial incision models have been formulated over the last 20 years, based on the early realization by *Gilbert* [1877] that sediment particles can be tools for bedrock erosion when they move and impact the river's bedrock, but can also provide a protective cover when they are resting, motionless, on the bed [e.g., *Kooi and Beaumont*, 1994; *Sklar and Dietrich*, 1998, 2001, 2004, 2006; *Turowski et al.*, 2007]. However, use and testing of such models remains extremely challenging at present because many of the sediment-related parameters are difficult to constrain, in particular grain size and lithology which strongly influence fluvial erosion rates [*Sklar and Dietrich*, 2001, 2004; *Gasparini et al.*, 2006, 2007; *Johnson et al.*, 2009] and are expected to evolve along actively incising rivers under the effect of abrasion, selective transport and lateral supply from hillslopes and tributaries [e.g., *Sklar et al.*, 2006; *Attal and Lavé*, 2006, 2009].

[5] The detachment-limited and transport-limited models are simple to parameterize using easily acquired field data and here we investigate how far they can be applied. These models have been implemented into models of landscape evolution such as the Channel-Hillslope Integrated Landscape Development (CHILD) model [*Tucker et al.*, 2001] and have proven successful at describing the evolution of bedrock rivers in the past (see above). We assess the extent to which these end-member fluvial incision models are able to replicate the exceptionally well constrained response of catchments in the central Apennines (Italy) to an increase in relative uplift rate. Unlike previous tests of fluvial erosion models which tend to focus on one single catchment [e.g., *Attal et al.*, 2008], this study is unique in that we simultaneously model the evolution of three monolithological catchments of different sizes (28 to 62 km^2) in the footwall of active normal faults which increased their throw rates to values ranging between 0.25 and 1.5 mm yr^{-1} around 0.75 Ma ago (Figure 1) [*Roberts and Michetti*, 2004]. In these catchments, channel and catchment morphology, the characteristics of the sediment supplied to and transported by the rivers, and the tectonic history of the faults have been extensively documented in the field [*Roberts and Michetti*, 2004; *Whittaker et al.*, 2007a, 2007b, 2008, 2010]. The wealth of constraints on the morphological and tectonic histories of these catchments as well as the differences in catchment size and bounding fault throw rates make them the ideal objects to test and calibrate fluvial erosion models, since a successful model should be able to replicate the evolution of the three catchments using a similar set of input parameters.

[6] We use the CHILD model [*Tucker et al.*, 2001] to simulate the evolution of the three catchments in response to an increase in fault throw rate. We include a slope-dependent channel width [*Finnegan et al.*, 2005] and calibrate the hydraulic scaling coefficients against field data to account for the channel narrowing which has been documented in the field as rivers steepen [*Whittaker et al.*, 2007a]. We perform tests using different values of a sediment entrainment (and erosion) threshold calibrated against field-derived fluvial sediment grain size to analyze the potential effect of sediment on landscape's response time and style [*Snyder et al.*, 2003a, 2003b; *Tucker*, 2004; *Lague et al.*, 2005]; in particular, we assess whether such a threshold could explain some of the key observations derived from field data such as a faster response with increasing relative uplift rate [*Whittaker et al.*, 2008]. After presenting the studied catchments and the modeling procedure, we present the results in the transport-limited and detachment-limited cases. We then discuss how these results improve our understanding of the response of the studied catchments in the Apennines and provide more generic guidelines on how to choose the best model to simulate the evolution of a given area and how to extract erosional and tectonic information from topography.

2. Study Area: Transient Catchments in the Apennines, Italy

[7] The three studied catchments are located in the central Apennines (Italy), an area which has been experiencing active extension for the last 3 Ma (Figure 1a) [*Roberts and Michetti*, 2004]. They are located in the footwall of active normal faults which accelerated ~0.75 Ma ago in response to fault linkage [*Roberts and Michetti*, 2004; *Whittaker et al.*, 2007a, 2007b]. All rivers are incising into Mesozoic platform limestone which shows little variation in Selby rock mass strength between and across catchments [*Whittaker et al.*, 2008].

[8] The Celano Gorge catchment occupies a 41 km^2 area in the footwall of the Fucino fault (Figure 1b). Where the river crosses the fault, the fault throw increased from 0.3 to 1.5 mm yr^{-1} 0.75 Ma ago [*Roberts and Michetti*, 2004; *Whittaker et al.*, 2007a, 2007b, 2008]. The Rio Torto and Torrente L'Apa catchments have drainage areas of 62 and 28 km^2, respectively, and both lie in the footwall of the

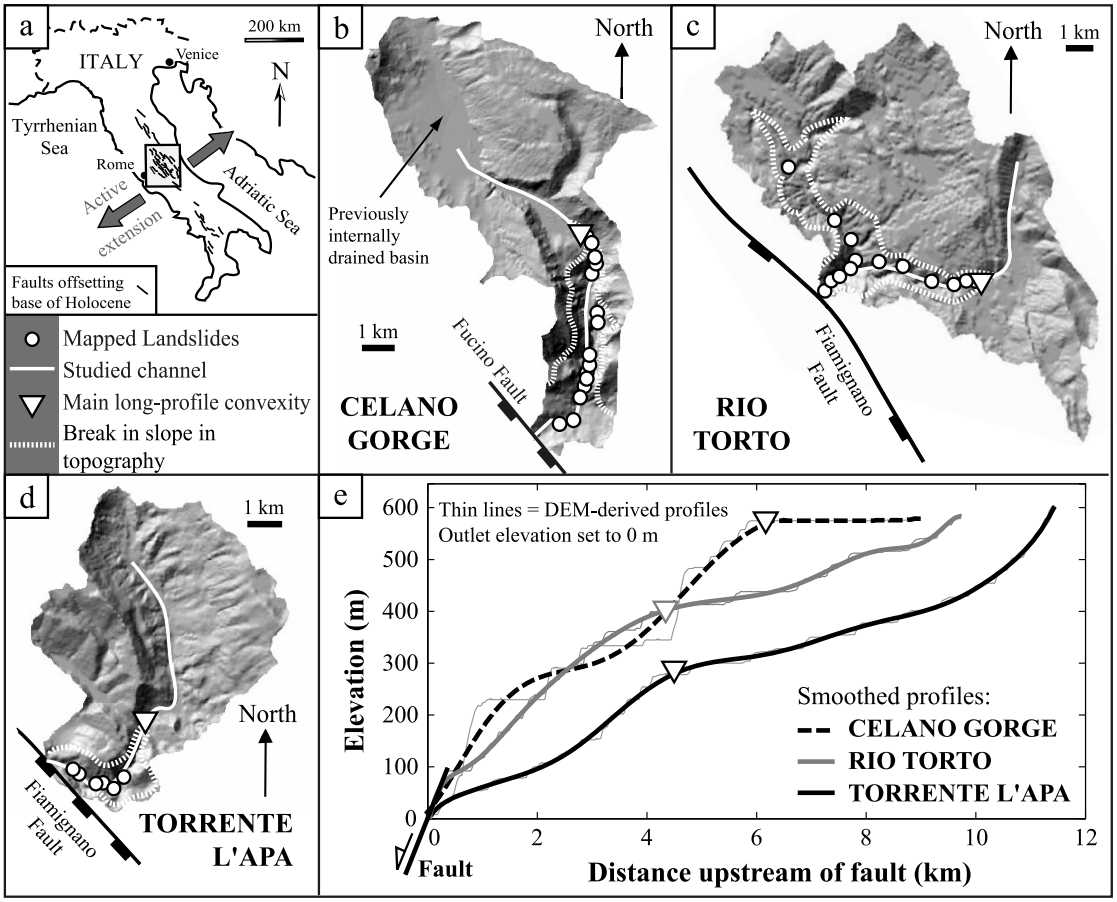

Figure 1. (a) Location map; box shows location of the central Apennines. Shaded topography of the (b) Celano Gorge, (c) Rio Torto, and (d) Torrente l'Apa catchments; mapped landslides, main long-profile convexities along the studied channels, and break in slope in topography delineating steepened landscape are shown. (e) River profiles extracted from the 20 m resolution DEM. Modified after *Whittaker et al.* [2010].

Fiamignano fault (Figures 1c and 1d). The Rio Torto crosses the fault in its center and experienced an increase in throw rate from 0.3 to 1 mm yr^{-1} ~0.75 Ma ago; the Torrente l'Apa crosses the fault near its eastern tip and experienced an increase in throw rate from 0.05 to 0.25 mm yr^{-1} ~0.75 Ma ago [*Roberts and Michetti*, 2004; *Whittaker et al.*, 2007a, 2007b, 2008]. The response of these catchments to fault acceleration is characterized by the development of a steepened, convex reach in the river long profile upstream of the fault (Figure 1e) while the upper part of the catchment is progressively uplifted and back tilted [*Whittaker et al.*, 2007a, 2007b, 2008; *Attal et al.*, 2008]. In the upper part of the catchments, channel slope is gentle and valleys are broad and open, with soil-mantled hillslopes. The lower part of the catchments exhibits steep channels, narrow gorges and steep coupled hillslopes near the angle of repose scarred by landslides delivering coarse material to the channel (Figure 1) [*Whittaker et al.*, 2007a, 2007b, 2008, 2010]. The two domains are separated by a prominent break in slope on the hillslope (Figures 1b–1d) and a major long-profile convexity along the rivers (Figure 1e). Downstream of the main long-profile convexity, river steepening is accompanied by a narrowing of the channel, leading to a breakdown of the typical square root relationship between discharge (or drainage area) and channel width [*Whittaker et al.*, 2007a]. Such channel adjustment has been shown to occur in many places worldwide in response to spatial or temporal variations in relative uplift rate and is now widely accepted [*Finnegan et al.*, 2005; *Stark*, 2006; *Wobus et al.*, 2006b; *Amos and Burbank*, 2007; *Whittaker et al.*, 2007a; *Attal et al.*, 2008; *Snyder and Kammer*, 2008; *Turowski et al.*, 2009; *Valla et al.*, 2010, *Yanites et al.*, 2010a; *Yanites and Tucker*, 2010]. Along the steepened reaches of the three channels, the width shows no clear downstream trend and is roughly constant: mean width values for the Celano Gorge, Rio Torto, and Torrente l'Apa are 7.4 ± 1.5, 9.5 ± 2.0, and 13.1 ± 2.8 m, respectively. The channel morphology along the steepened reaches is characterized at the reach scale by more or less prominent steps and pools alternating with relatively steep bedrock reaches with discontinuous sediment cover; bedrock exposure is high, typically >50% [*Whittaker et al.*, 2007b]. Bedrock is often exposed on the channel bed and its morphology (smooth surfaces, flutes,

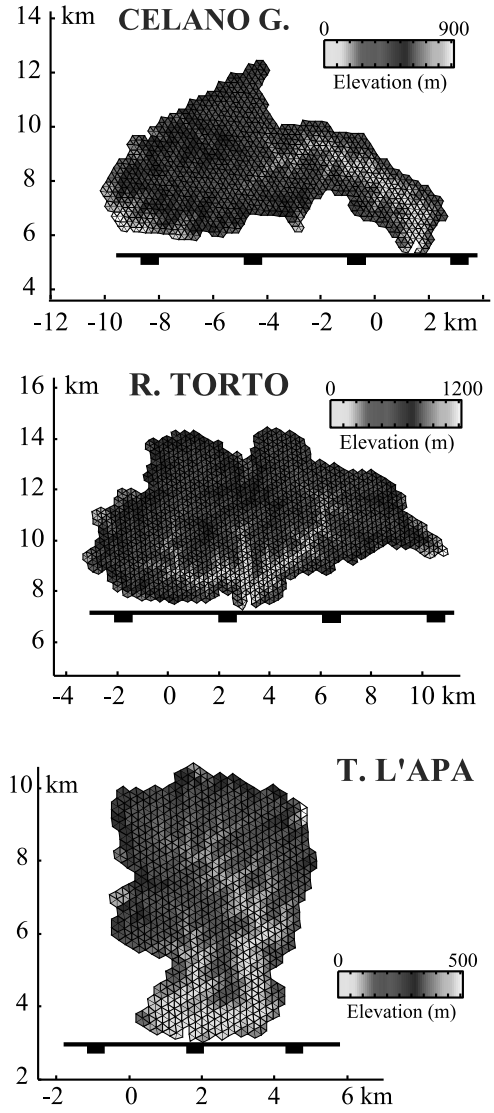

Figure 2. Modeled topographies in steady state with the uplift rate prior to fault acceleration for the three studied catchments. Uplift rate decreases linearly from fault to the fulcrum located 10 km away from the fault. Node spacing is ~200 m. In this case, τ_c = 0 Pa (see text).

potholes) demonstrates that abrasion is the dominant bedrock erosion process.

3. Modeling the Transient Response of the Studied Catchments

3.1. Model Setup

[9] The CHILD model [*Tucker et al.*, 2001] is used to model the evolution of the Italian catchments. The procedure is similar to that used by *Attal et al.* [2008] to investigate the impact of channel width adjustment on the evolution of the Rio Torto catchment and readers are referred to that paper for a full treatment of the approach. In brief, the topography of the three catchments was extracted from a 20 m resolution digital elevation model (DEM) and transformed into a Triangulated Irregular Network (TIN) with an average node spacing of 200 m (Figure 2). The use of the block-tilting model (rather than an elastic dislocation model [e.g., *Ellis et al.*, 1999]) is justified in the central Apennines by the small spacing between faults [*Anders et al.*, 1993], on average 10 km [*Roberts and Michetti*, 2004]. We applied a rock uplift rate to the catchments which was greatest at the fault and decreased linearly to zero from fault to fulcrum, the latter being positioned 10 km away from the fault to reflect the average fault spacing [*Attal et al.*, 2008].

[10] In CHILD, rainfall is uniform over the modeled landscape and is generated according to a Poisson rectangular pulse rainfall model [*Eagleson*, 1978; *Tucker and Bras*, 2000]. The values used for mean storm precipitation rate (0.75 mm h^{-1}), mean storm duration (22 h) and mean interstorm duration (260 h) are typical of a Mediterranean-style climate, based on data from the U.S. west coast [*Hawk*, 1992; *Attal et al.*, 2008]. In the absence of detailed constraints on the changes to these specific climate parameters over the Quaternary, the parameters were kept constant during all runs.

[11] Field data show a clear correlation between channel width and gradient: channels tend to narrow as they steepen, leading to channels along the steepened reaches that are narrower than predicted by the conventional hydraulic scaling relationship (section 2). *Finnegan et al.* [2005] proposed a relationship which accounts for such a channel adjustment

$$W = k_w Q^{3/8} S^{-3/16}, \tag{1}$$

where W is channel width, k_w is a constant, Q is discharge and S is channel slope. This relationship significantly improves the prediction of channel width along the studied rivers [*Whittaker et al.*, 2007a; *Attal et al.*, 2008] and is supported by a simple physically based models of self-formed bedrock channels [*Wobus et al.*, 2006b; *Turowski et al.*, 2009; *Yanites and Tucker*, 2010]. We therefore use equation (1) to calculate channel width across the modeled landscapes.

[12] *Whittaker et al.* [2007b] estimated that ~2 Ma would be required for catchments in the Apennines to achieve steady state. Fault initiation occurred 3 Ma ago and fault acceleration 0.75 Ma ago: this implies that the catchments had achieved steady state with respect to the uplift field prior to fault acceleration. In this study, we assume that the drainage patterns and catchment boundaries have not changed since fault acceleration. For all runs, the modern TINs of the three catchments were entered into CHILD and the model was run with the uplift field prior to fault acceleration (fault throw = 0.3 mm yr^{-1} for Celano Gorge and Rio Torto, 0.05 mm yr^{-1} for Torrente l'Apa) until steady state was reached. Starting from these steady state topographies (Figure 2), the morphological response of the catchments to fault acceleration (fault throw = 1.5, 1.0, and 0.25 mm yr^{-1} for Celano Gorge, Rio Torto, and Torrente l'Apa, respectively) was then analyzed.

[13] Note that field and DEM observations show that the upper part of the Celano Gorge catchment was an internally drained basin which has been captured by the main river (Figure 1b). We chose to include the previously internally drained basin into the modeled catchment because field evidence indicates that capture happened before fault acceleration and that this basin should thus be contributing

water to the Celano Gorge in our modeling of the catchment's response to fault acceleration. Evidence for an early capture includes: the fact that the prominent rock ridge which was breached, probably through regressive erosion, is ~3 km upstream of the main long-profile convexity (Figure 1b) and that the channel slope between the ridge and this convexity is extremely low, <0.002 (Figure 1e). Previous modeling work [*Attal et al.*, 2008] showed that once fault acceleration has commenced, capture by the low gradient reaches upstream of the migrating long-profile convexity is unlikely. In the following, we will focus our comparison of catchment morphology and river profiles to the part downstream of the prominent ridge located ~9 km upstream of the fault (Figure 1e).

3.2. Fluvial Erosion Models

[14] In the detachment-limited model, fluvial erosion E is calculated at all points in the modeled landscape according to

$$E = k_b(\tau - \tau_{ce})^p \text{ for } \tau > \tau_{ce}, \tag{2a}$$

$$E = 0 \text{ for } \tau \leq \tau_{ce}, \tag{2b}$$

where k_b is the erodibility coefficient, p is a constant, τ is the fluvial shear stress and τ_{ce} is a threshold representing the shear stress that must be exceeded for erosion to happen. We consider that the rate of incision is proportional to the rate of energy dissipation per unit bed area and set p to 3/2 [*Seidl and Dietrich*, 1992; *Howard et al.*, 1994; *Whipple and Tucker*, 1999, *Attal et al.*, 2008]. By assuming steady, uniform flow in a relatively wide channel and applying Manning's roughness formula, we calculate the cross-section averaged boundary shear stress as

$$\tau = \rho g n_m^{3/5} (Q/W)^{3/5} S^{7/10}, \tag{3}$$

where Q is the water discharge, W is the channel width (calculated following equation (1)), S is channel slope, ρ is the water density (1000 kg m^{-3}), g is the gravitational acceleration and n_m is the Manning's roughness coefficient, fixed to 0.03 in this study, a common value used for rivers transporting sediment up to cobble size (for derivation, see, e.g., *Howard* [1994]). Note that when $\tau_{ce} = 0$, equation (2) is equivalent to the linear SSP model. When in addition the exponent p is set to 1, equation (2) is equivalent to the linear shear stress model. For simplicity and in the absence of constraint on the amount of water intercepted by vegetation, lost by evaporation, and on the infiltration capacity of the soils in the study area, we calculate the discharge Q as the product of the precipitation rate by the drainage area. This will tend to overestimate Q but should not affect the comparison between catchments and models since the same calculation method was applied to all runs.

[15] In the transport-limited model, erosion at any point in the landscape is calculated following:

$$E = \frac{1}{W}\frac{\partial Q_s}{\partial \vec{x}}, \tag{4}$$

where Q_s is the sediment flux and $\vec{x}$ represents the distance in the downstream direction. The ratio $\partial Q_s/\partial \vec{x}$ thus represents the divergence of the sediment flux in the downstream direction: if the amount of sediment exiting a given point is higher than the amount of sediment entering this point, this term is positive and the river erodes; in the opposite case, deposition occurs. In a transport-limited system, the river is "at capacity": sediment is always available and the sediment flux Q_s equals the transport capacity Q_c. Transport capacity is calculated following:

$$Q_c = k_f W (\tau - \tau_{ct})^{p'}, \tag{5}$$

where k_f is a free transport efficiency coefficient, p' is a constant (set to 3/2), τ is the fluvial shear stress calculated following equation (3) and τ_{ct} is a threshold representing the shear stress that must be exceeded for sediment transport to happen ($Q_c = 0$ if $\tau < \tau_{ct}$). Previous studies showed that a threshold is required to produce realistic transport-limited landscapes characterized by concave up river profiles [e.g., *Tucker and Whipple*, 2002; *Tucker*, 2004]. In this study we therefore set $\tau_{ct} > 0$ for all transport-limited runs.

3.3. Calibration

[16] The data collected in the field allows the calibration of three constants: the channel width prefactor k_w (equation (1)), the erodibility coefficient k_b (equation (2)) and the thresholds for erosion and sediment transport τ_{ce} and τ_{ct} (equations (2) and (5)). The threshold for erosion τ_{ce} can be interpreted in two ways: it can represent the shear stress value that must be exceeded either for bedrock detachment to occur (bedrock-controlled threshold) or for setting tools in motion and exposing bedrock (sediment-controlled threshold) [e.g., *Howard*, 1994; *Lavé and Avouac*, 2001; *Sklar and Dietrich*, 2004]. Progress has been made recently on the quantification of the shear stress required for plucking blocks from heavily jointed bedrock [e.g., *Whipple et al.*, 2000b; *Chatanantavet and Parker*, 2009]. However, *Sklar and Dietrich*'s [2001] experiments suggest that the "bedrock-controlled" threshold "can be neglected in the case of bed load abrasion because even the relatively low-impact energy of fine sand moving as bed load is sufficient to cause measurable bedrock wear" [*Sklar and Dietrich*, 2004]. Because field observations in the studied catchments indicate that abrasion by bed load is the dominant bedrock erosion process [*Whittaker et al.*, 2007b], we focus on the "sediment-controlled" threshold. This threshold can be estimated using the Shields criterion (see *Buffington and Montgomery* [1997] for a review on the application of this method) and the grain size of the sediment transported by rivers. Note that this type of threshold for bedrock erosion τ_{ce} has the same significance that the threshold for sediment transport τ_{ct}: in the former case, the threshold must be exceeded for sediment to be put in motion, thus exposing bedrock and providing tools for erosion; in the later case, the threshold must be exceeded for sediment transport to happen. In the following, we will thus refer to both erosion and transport thresholds using a single "sediment-controlled" threshold term τ_c.

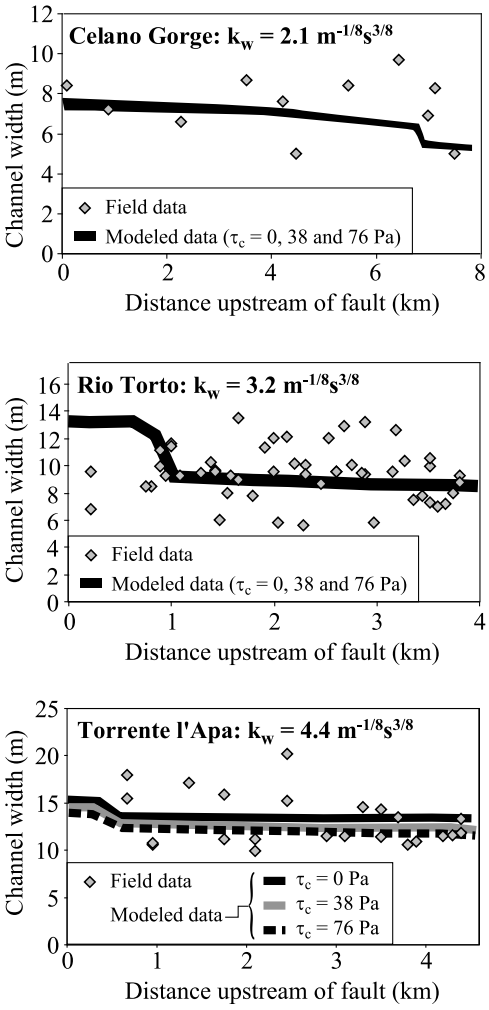

Figure 3. Comparison of modeled channel width with field data along the steepened reaches (between the fault and the main long-profile convexity) for the three rivers studied, in the detachment-limited case, for a representative storm with a precipitation rate of 0.75 mm h^{-1}. Calculation of modeled width is made at the time after fault acceleration at which the position of the modeled long-profile convexity coincides with the position of the real convexity (see section 3.4 and Figure 5 for a description of the transient response). Values of k_w are given for each river. Note the changes in scale on x and y axes.

[17] The critical shear stress for particle entrainment can be calculated using

$$\tau_c = \tau_c^*.\Delta\rho g D, \quad (6)$$

where τ_c^* is the dimensionless critical shear stress (Shields stress) commonly assumed to be ~0.045 for turbulent rough flows [*Buffington and Montgomery*, 1997], $\Delta\rho$ is the difference in density between the fluid and the sediment (1650 kg m^{-3} for typical crustal rocks) and D is a grain size representative of the sediment, usually taken as the median grain size. Along the steepened reaches of the three studied rivers, the grain size distributions are roughly similar [*Whittaker et al.*, 2007b, 2010]. In particular, sieving of volumetric samples yielded median grain sizes D_{50} of ~50 mm and minimum D_{84} (84th percentile characterizing the coarse fraction) of ~100 mm. The threshold shear stresses calculated using these two grain sizes are τ_c = 38 and 76 Pa, respectively. Whereas this simplistic approach ignores the imbrication and hiding effects that exert an important control on sediment's incipient motion in mountain rivers [e.g., *Yager et al.*, 2007], we believe that the shear stress to mobilize grains of diameter $D = D_{84}$ calculated using equation (6) (τ_c = 76 Pa) represents in first approximation the upper limit for the shear stress that would be required to put the sediment in motion in the studied catchments. In the following, we present the results of detachment-limited runs using τ_c = 0, 38 and 76 Pa, and transport-limited runs using τ_c = 38 and 76 Pa.

[18] Equation (1) implies that the channel width coefficient k_w can be calculated if width, slope, and discharge are known at a point along the channel for a particular flow stage. We used the width and slope values measured in the field along the steepened reaches of the three catchments and estimated the discharge for a representative storm with a precipitation rate of 0.75 mm h^{-1}, similar to the average precipitation rate used in CHILD. The k_w values obtained for the Celano Gorge, Rio Torto, and Torrente l'Apa are 2.1, 3.2, and 4.4 $m^{-1/8}$ $s^{3/8}$, respectively. In the model, steepened reaches are produced in response to an increase in uplift rate (see section 3.4) [*Attal et al.*, 2008]. Along these steepened reaches, a good agreement is found between modeled channel width using the k_w values above and the channel width measured in the field (Figure 3).

[19] To calibrate the erodibility coefficient k_b in the detachment-limited model, we use the Rio Torto catchment, which has been studied in the field in considerable detail [*Whittaker et al.*, 2007a, 2007b, 2008, 2010; *Attal et al.*, 2008]. For each value of τ_c, k_b was set to produce a steepened reach with an average slope of 0.1, matching the slope of the real steepened reach (Figure 1e). The values of k_b obtained for τ_c = 0, 38, and 76 Pa are 5.2, 7.5, and 12.0 × 10^{-6} m $Pa^{-3/2}$ yr^{-1}, respectively: the higher the threshold, the lower the river's erosive efficiency, so the higher the erodibility coefficient required to have a river with the same slope eroding at the same rate [*Attal et al.*, 2008]. We emphasize that because the rivers in the three catchments incise the same type of rock and transport sediment with similar characteristics, the same value of k_b was used in the three catchments for each value of τ_c. The most successful pair of k_b/τ_c values will thus be the one that produces the best fit in terms of topography for all three catchments. The different parameters used in the runs are summarized in Table 1.

[20] Finally, the transport efficiency coefficient k_f (equation (5)) is a free parameter in the transport-limited case. We performed a series of tests to define the range of k_f values that produce topographies which could realistically be compared to the real topographies. In this section, we present the results of runs using k_f values varying between 10 and 300 m^2 $Pa^{-3/2}$ yr^{-1}.

3.4. Model Results

[21] In this section, the modeled evolution of the three catchments' trunk river profiles (Figure 1) in response to an increase in slip rate is analyzed. In each case (transport

Table 1. Summary of the Parameters Used in the Model

Parameter	Value
Average node spacing	200 m
Mean precipitation rate	0.75 mm h^{-1}
Mean storm duration	22 h
Mean interstorm duration	260 h
Manning's bed roughness coefficient n_m	0.03
Channel width coefficient k_w, Celano Gorge	2.1 $m^{-1/8}$ $s^{3/8}$
Channel width coefficient k_w, Rio Torto	3.2 $m^{-1/8}$ $s^{3/8}$
Channel width coefficient k_w, Torrente l'Apa	4.4 $m^{-1/8}$ $s^{3/8}$
Erodibility coefficient k_b, τ_c = 0 Pa	$5.2.10^{-6}$ m $Pa^{-3/2}$ yr^{-1}
Erodibility coefficient k_b, τ_c = 38 Pa	$7.5.10^{-6}$ m $Pa^{-3/2}$ yr^{-1}
Erodibility coefficient k_b, τ_c = 76 Pa	12.10^{-6} m $Pa^{-3/2}$ yr^{-1}

limited and τ_c = 38, 76 Pa; detachment limited and τ_c = 0, 38, 76 Pa), the initial profiles in steady state with the slip rate prior to fault acceleration and the transient profiles are displayed. The modeled profiles are compared to the real profiles extracted from the DEM (Figures 4 and 5).

3.4.1. Transport-Limited Case

[22] In all transport-limited cases (τ_c = 38, 76 Pa) and for all three catchments, the response of the topography to an increase in uplift rate is characterized by a general steepening of the whole catchment, irrespective of the uplift rate after fault acceleration or the k_f value used. This behavior is consistent with the transient response documented by *Whipple and Tucker* [2002] in their numerical modeling study (Figure 4a). As expected, the threshold τ_c influences the steepness of both initial steady state profiles and transient profiles (Figures 4b and 4c): the higher the threshold, the steeper the slope required to move a given amount of sediment. Similarly, the transport efficiency coefficient k_f also affects the landscape's steepness (Figures 4b and 4c): the higher the transport efficiency, the lower the slope required to move a given amount of sediment. Initial steady state profiles are concave up for all values of k_f (gray zone in Figures 4b and 4c). For most values of k_f (40 to 300 m^2 $Pa^{-3/2}$ yr^{-1}), channel steepening after fault acceleration is modest: the profiles generated 1 Ma after fault acceleration are concave up and are at steady state with respect to the new uplift field (Figures 4b and 4c). Their slopes are far from matching the slope along the steepened reach of the real catchment. For the lowest values of k_f however (10–20 m^2 $Pa^{-3/2}$ yr^{-1}), the increase in uplift rate leads to a substantial steepening of the profiles: 1 Ma after fault acceleration, the general slope of the profile produced with k_f = 10 m^2 $Pa^{-3/2}$ yr^{-1} is similar to the slope along the steepened reach of the real profile (Figures 4b and 4c). For both values of k_f, steady state is not reached and the channels carry on steepening 1 Ma after fault acceleration. The transient response is accompanied by the development of a gentle convexity in these runs simulating a landscape where rivers are not very efficient at transporting sediment. However, this convexity is much more subdued than the one observed in the real catchment. Similar observations were made in the two other studied catchments. These results indicate that the transport-limited model does not provide a good fit to the real data, even with the inclusion of an appropriate threshold (see discussion).

3.4.2. Detachment-Limited Case

3.4.2.1. River Profiles

[23] In the detachment-limited case, profiles in steady state with the uplift rate prior to fault acceleration (thin lines) are all concave up. An increase in rock uplift rate leads to the development of a long-profile convexity propagating upstream [*Whipple and Tucker*, 2002; *Attal et al.*, 2008]: downstream of the convexity, the steepened landscape has adjusted to the new uplift field; upstream of the convexity, the landscape has not "felt" yet the change in uplift rate and is progressively uplifted and back tilted [*Attal et al.*, 2008]. Below, we compare the best fit profiles obtained in terms of location of the long-profile convexity upstream of fault (Figure 5). To locate the main convexity, the curvature was calculated along the real and modeled profiles: the main long-profile convexity was assumed to correspond to the point of maximum curvature along the profile.

[24] In all three catchments, increasing the threshold for erosion τ_c leads to steeper landscapes, prior to and after fault acceleration (Figure 5) [*Attal et al.*, 2008]. The erodibility coefficient k_b was calibrated for each τ_c value to produce a steepened reach matching the steepened reach of the Rio Torto (section 3.3 and Figure 5b). For this catchment, the best fit in terms of location of long-profile convexity is obtained 0.45 Ma after fault acceleration for τ_c = 0. In this scenario, the modeled profile also fits the shape of the real profile upstream of the convexity [*Attal et al.*, 2008]. Increasing the threshold τ_c leads to an oversteepening of the profile upstream of the convexity and a best fit profile (in terms of location of the convexity) produced earlier, 0.35 and 0.25 Ma after fault acceleration for τ_c = 38 and 76 Pa, respectively. Such change in timing is partly due to the fact that the propagation rate of long-profile convexities is a function of bedrock erodibility [*Rosenbloom and Anderson*, 1994; *Attal et al.*, 2008] and that the higher the threshold, the higher the erodibility coefficient required to have the river eroding at the same rate with similar slopes (section 3.3).

[25] The introduction of a threshold for erosion has only a modest effect on the modeled profile of the Celano Gorge (Figure 5a) because this catchment is experiencing the highest uplift rate of all three catchments: shear stress along the river has to be relatively high to produce erosion rates matching the uplift rate and the likelihood of floods with shear stresses in excess of the threshold for erosion along this river is thus relatively high compared to catchments experiencing low uplift rates such as the Torrente l'Apa. In this latter catchment, varying τ_c has little impact on the timing of the response (best fit obtained 0.75–0.8 Ma after fault acceleration for all values of τ_c) but leads to markedly different profiles (Figure 5c). In the Celano Gorge, the location of the long-profile convexity is quite well predicted in terms of distance from fault but also elevation, for all values of τ_c (Figure 5a). However, the best fit profiles for the Celano case are produced between 0.35 and 0.5 Ma after fault acceleration for all values of τ_c. Downstream of the convexity, the predicted steepened reach has a roughly constant slope, in contrast to the real profile which shows secondary convexities. Upstream of the convexity, the presence of a previously internally drained basin ("old

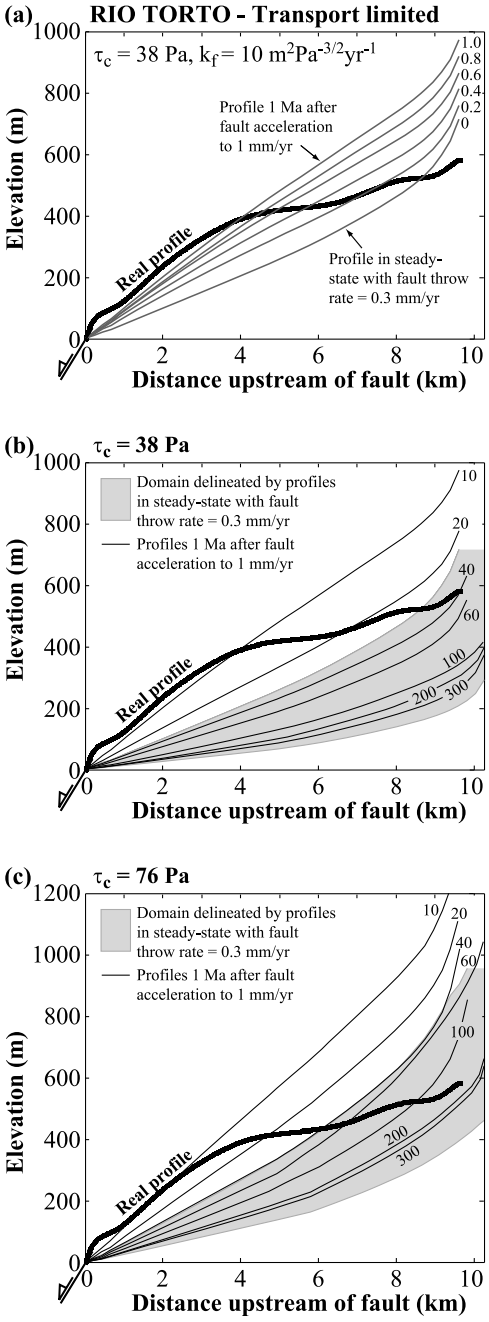

Figure 4. Comparison of modeled profiles using the transport-limited fluvial erosion law with the DEM-derived profile for the Rio Torto. The thickest black line is the real profile. (a) Profile evolution after fault acceleration to 1 mm yr^{-1}. In this case, τ_c = 38 Pa and k_f = 10 m^2 $Pa^{-3/2}$ yr^{-1}. Profiles are displayed every 0.2 Ma (time after acceleration is indicated for each profile in Ma). Initial profiles and profiles 1 Ma after fault acceleration with τ_c = (b) 38 and (c) 76 Pa for different values of k_f. The domain delineated by the initial profiles in steady state with the uplift rate prior to fault acceleration is the shaded zone: the top and the bottom of this zone are the profiles obtained with the lowest and highest values of k_f, respectively. Values of k_f are indicated on profiles 1 Ma after fault acceleration (in m^2 $Pa^{-3/2}$ yr^{-1}). Differences in overall profile shape are due to the river following slightly different paths in some cases.

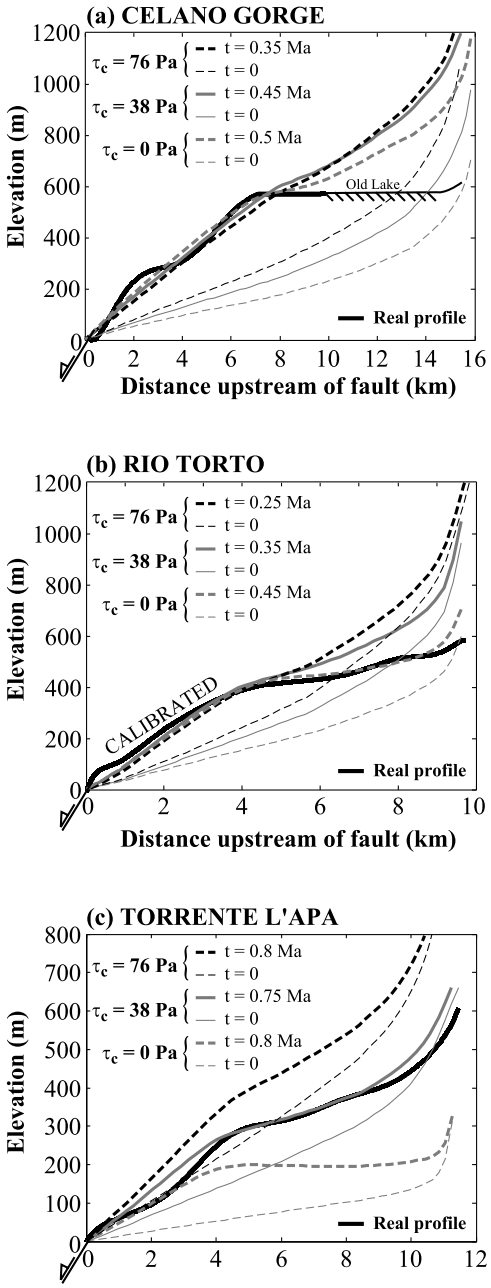

Figure 5. Comparison of modeled profiles using the detachment-limited fluvial erosion law with the DEM-derived profiles for the three studied rivers: (a) Celano Gorge, (b) Rio Torto, and (c) Torrente l'Apa. The thick solid black line is the real profile. Modeled profiles obtained using τ_c = 0, 38, and 76 Pa are the dashed gray, solid gray, and dashed black lines, respectively. Initial profiles (t = 0) in steady state with uplift rate prior to fault acceleration are thin lines in each case. Thick lines in each case represent the best fit to the real profile in terms of location of the main long-profile convexity (time after fault acceleration for best-fit profiles is indicated). Erodibility coefficient is calibrated using the slope along the steepened reach of the Rio Torto, thus explaining the fit between modeled and real profile in all cases in Figure 5b. Note the change in scale on x and y axes.

lake") precludes the comparison of the profiles more than 9 km upstream of the fault (see section 3.1). Between the main convexity and this "9 km" limit, the real profile is very shallow (<0.002) and all predicted profiles are too steep, even if the profile predicted with no threshold shows a noticeable leveling of the elevation upstream of the convexity, between 7 and 8.5 km upstream of the fault. For the Torrente l'Apa, the profile predicted with no threshold matches well the lower part of the steepened reach (up to 2.5 km upstream of the fault) but produces a too shallower profile overall, with a long-profile convexity at an elevation ~100 m lower than the real convexity (Figure 5c). The profile produced using τ_c = 38 Pa matches well the location of the main convexity (distance from fault and elevation), as well as the profile upstream of the convexity. However, the model predicts a roughly constant slope downstream of the convexity and fails to reproduce the lower slopes exhibited by the real profile immediately upstream of the fault. The overall slopes predicted by the run with τ_c = 76 Pa are far too steep across the whole catchment (Figure 5c).

3.4.2.2. Timing of the Response

[26] One way of quantitatively assessing the response time of detachment-limited systems is to analyze the retreat rate of the main long-profile convexity. According to the SSP model, this rate can be approximated as $\psi A^{0.5}$, where A is the drainage area and ψ is a constant (in year^{-1}), all other variables being equal [*Tucker and Whipple*, 2002; *Crosby and Whipple*, 2006; *Wobus et al.*, 2006c]. The time t required to propagate a convexity over a distance L is therefore

$$t = L/\psi A^{0.5}. \quad (7)$$

Following *Whittaker et al.*'s [2008] method, we calculate the parameter ψ for all our runs. The parameter is calculated iteratively to account for changes in drainage area as the convexity propagates upstream: the reach between the fault and the convexity is divided into segments along which drainage area does not vary significantly (in our case, each segment corresponds to the section of the modeled profile between each node and its downstream neighbor). For each segment of length L_i with a corresponding drainage area A_i, the time t_i required to propagate the convexity through it is calculated as $t_i = L_i/\psi A_i^{0.5}$. The coefficient ψ is then adjusted until the sum of the t_i equals the duration of the run (time after fault acceleration). The results show that even with no threshold, the ψ parameter strongly depends on uplift rate, as observed in the field (Figure 6) and discussed below (section 4.1.3). This modeling result is due to the channel width dependency on slope (equation (1)) and differences in the prefactor k_w between catchments (see section 3.3): test runs using the typical hydraulic scaling relationship (width scales with the square root of drainage area [*Leopold and Maddock*, 1953]), a constant value of k_w and no threshold yielded similar values of ψ for all three catchments, consistent with predictions derived from the linear versions of the detachment-limited model. Increasing the threshold value τ_c leads to a larger increase in ψ with increasing uplift rate but has a minor effect on the Torrente l'Apa's result: within error, the ψ value obtained is similar to the one obtained from the analysis of the real profile (Figure 6) [*Whittaker et al.*, 2008]. Whereas the predicted retreat rate of the convexity matches the retreat rate estimated from the real data for Torrente l'Apa (Figures 5c and 6), it is far too high for the two other catchments: in both catchments, the main convexity propagates too fast and the best fit in terms of location of the long-profile convexity is achieved too early after fault acceleration. Increasing the threshold should slow down the response by reducing the frequency of erosive floods. However, the erodibility coefficient k_b has to be increased when increasing the threshold to fit the steepened reach along the profile of Rio Torto (see section 3.3). Increasing k_b speeds up the response and this effect is dominant here: increasing the threshold (and k_b) makes the timing worse (Figures 5a, 5b, and 6).

4. Discussion

4.1. Insights Into the Evolution of the Studied Catchments in the Apennines

4.1.1. Best Model for the Evolution of the Studied Catchments

[28] The runs with the transport-limited fluvial erosion model (section 3.4.1) show that very low values of the transport efficiency coefficient k_f, that is, values more than 1 order of magnitude lower than the values of 400–500 m^2 Pa$^{-3/2}$ yr^{-1} typically found in gravel bed rivers [*Meyer-Peter and Müller*, 1948], are required to produce landscapes as steep as those observed in the field. This result is in agreement with studies of sediment transport in steep mountain rivers which typically show that conventional transport equations such as *Meyer-Peter and Müller*'s [1948] lead to an overestimation of the measured transport rates by orders of magnitude [e.g., *Rickenmann*, 2001; *Yager et al.*, 2007]. However, in most of our runs ($k_f \geq$ 40 m^2 Pa$^{-3/2}$ yr^{-1}), the response of the landscape to fault acceleration is diffuse and produces low-relief landscapes and no long-profile convexity (Figure 4). In the Rio Torto case, values as low as 10 m^2 Pa$^{-3/2}$ yr^{-1} are necessary to produce a steepened reach as steep as the observed one in less than 1 Ma after fault acceleration. In this case, the evolution is characterized by an overall steepening of the landscape and a slow increase in erosion rate. River incision is limited due to the low transport capacity of the rivers: the topography is poorly dissected and there is no sharp transition between upper and lower catchment, contrary to what is observed in the field. This is also true for the river profile: a convexity appears on the profile for such low value of the k_f coefficient but it is much more subdued than in reality (Figure 4). Changing the threshold value does not make a significant difference to these observations. The inability of the transport-limited fluvial erosion model to produce profile convexities in response to fault acceleration, regardless of how it is parameterized, suggests that this model is not suitable to model the evolution of the studied catchments in the Apennines [*Whittaker et al.*, 2008].

[29] The detachment-limited model on the other hand produces profiles that have many similarities with the observed real profiles. In particular, a threshold value of 38 Pa (derived using the median grain size D_{50} in the studied catchments) is the only threshold value that produces a reasonable fit of both the distance along stream and elevation of the main convexity along all three rivers, using the same set of input parameters (Figure 5). Although these best

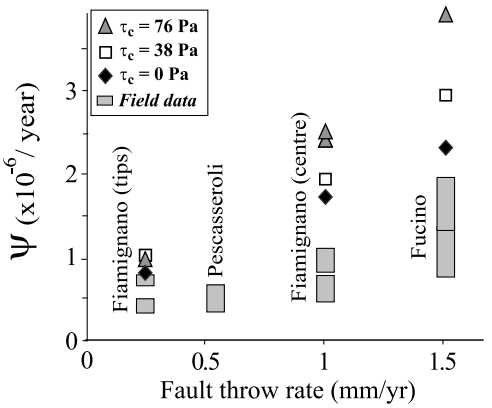

Figure 6. Comparison of modeled and field-derived values of the migration rate of long-profile convexities ψ as a function of fault throw rate after acceleration for rivers crossing tthree active normal faults that have accelerated ~0.75 Ma ago: the Fiamignano, Pescasseroli, and Fucino faults (modified after *Whittaker et al.* [2008]). The modeled values are given for the Torrente l'Apa (tip of the Fiamignano fault), the Rio Torto and its main tributary (center of the Fiamignano fault), and the Celano Gorge (Fucino fault).

fitting modeled long profiles imply times since fault acceleration generally less than observed in the field (i.e., ≤0.75 Ma), the mismatch is reduced for lower values of τ_c. This result is mostly constrained by Torrente l'Apa, the catchment that is the most sensitive to the introduction of a threshold: in this catchment, relative uplift rates and thus erosion rates and stream power are generally lower than in the two other catchments and the likelihood of having floods generating shear stresses in excess of the critical shear stresses is therefore lower than in the two other catchments. Using a threshold of 0 or 76 Pa produces a convexity 100 m below or above, respectively, the position of the actual convexity along the Torrente l'Apa profile (Figure 5c). For the Celano Gorge and Rio Torto, the location of the main long-profile convexity is reasonably fitted using any of the threshold values investigated in this study (0, 38 and 76 Pa).

4.1.2. Significance of the Threshold for Erosion

[30] Whereas a threshold value of 38 Pa produces a good fit for the three catchments in terms of the location of the main profile convexity, it generates unrealistically steep landscapes for Rio Torto and Celano Gorge upstream of the convexity (Figures 5a and 5b). In the Rio Torto case, the run with no threshold produces the best fit for the upper profile. In the Celano Gorge, the run with no threshold is the only one to produce a noticeable leveling of the profile (between 7 and 8.5 km upstream of the fault), as observed in the field between the main convexity and the old lake (Figure 5a). One can question the use of a single catchment-wide value of the threshold τ_c in these transient landscapes. Previous work in varied landscapes and contrasted climatic settings showed that differences in slope steepness are associated with differences in hillslope processes: as gradient increases, shallow hillslope erosion processes, e.g., ravelling and creeping, are replaced by deep-seated landslides, rockfalls and formation of large scree cones [*Burbank et al.*, 1996, *Roering et al.*, 1999, *Lavé and Burbank*, 2004]. More specifically, *Whittaker et al.* [2008, 2010] showed that the steepening of the landscape in response to an increase in relative uplift rate in the Apennines is accompanied by changes in hillslope erosion processes that lead to changes in fluvial sediment grain size distribution (Figure 7): along the steepened reaches, steep coupled hillslopes supply coarse sediment through landsliding, whereas sediment supply from soil-mantled hillslopes remains fine grained in the upper catchment. As a result, sediment tends to be coarser along the steepened reaches than upstream of the main long-profile convexity (Figure 7b). Because we believe that the threshold for erosion represents the shear stress required to put sediment in motion in our context (see section 3.3), this threshold should be higher along the steepened reach than upstream of the convexity. Further work on the feedbacks between uplift, hillslope erosion and sediment supply to mountain rivers will be required to design a more realistic threshold for sediment motion taking into account variations in fluvial sediment caliber induced by changes in slope steepness and/or hillslope erosion processes. Note that in the Torrente l'Apa case, a constant τ_c = 38 Pa replicates both the location of the long-profile convexity and the shape of the upper profile. This could be due to the relative uplift rate in this catchment being the lowest of all three catchments: the increase in uplift rate has led to a relatively modest steepening of the landscape and thus to a more subtle increase in grain size along the steepened reach [*Whittaker et al.*, 2010]. In this case, a single catchment-wide value of τ_c may be appropriate to simulate the evolution of this catchment.

4.1.3. Landscape Response Time and Channel Narrowing

[31] *Whittaker et al.*'s [2008] study of a series of catchments in the Apennines revealed an increase in long-profile convexity migration rate with increasing relative uplift rate (Figure 6). This was a key observation that they suggested might be explained either by (1) a stronger slope dependence in the detachment-limited erosion model ($p > 1$; equation (2)), (2) a nonzero erosion threshold ($\tau_c > 0$), or (3) an explicit role for sediment in enhancing erosion rates by providing tools that impact/abrade bedrock [e.g., *Whipple and Tucker*, 2002; *Gasparini et al.*, 2007]. Our model results show that in fact a slope-dependent channel width (equation (1)) and a varying prefactor k_w produce an increase in the migration rate of long-profile convexities with increasing uplift rate in the detachment-limited case, even without threshold for erosion (section 3.4.2.2 and Figure 6). Invoking stronger slope dependence is also not required. Such variation in migration rate is expected using our approach, as equations (2) and (3) can be combined and rewritten as follows, for $\tau_c = 0$:

$$dz/dt \propto (Q/W)^{9/10}(dz/dx)^{\sim 1}, \tag{8}$$

where z is elevation, t is time and x is long-profile distance. This is a wave equation in which the wave speed is proportional to $(Q/W)^{9/10}$. Narrower channels are thus expected to respond faster to a disturbance [e.g., *Attal et al.*, 2008]. Here, channel width is calculated according to equation (1): it increases with discharge and decreases with slope. Because channels steepen when relative uplift rate increases, then the higher the uplift rate after fault acceleration, the higher the amount of narrowing experienced by the chan-

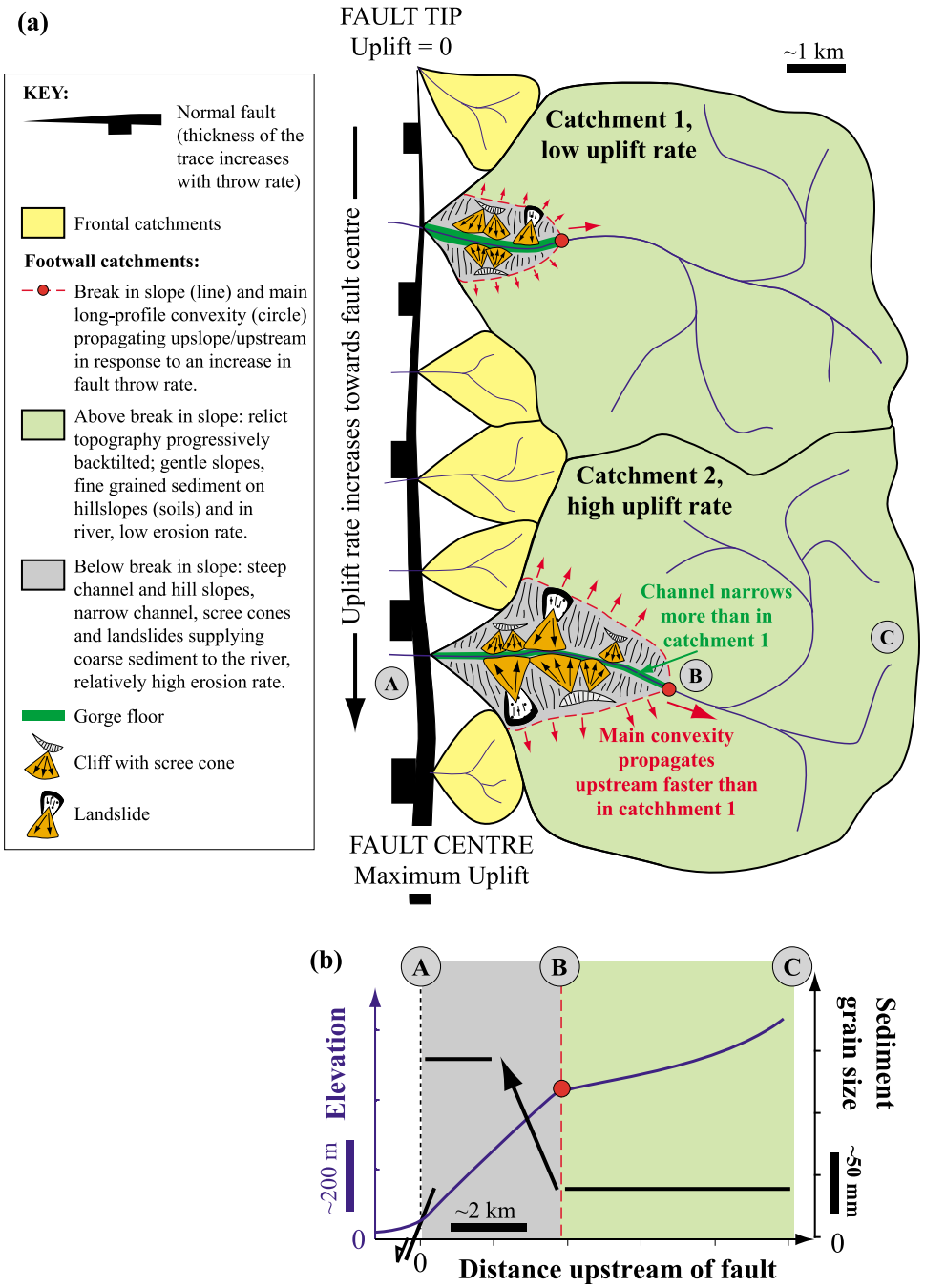

Figure 7. (a) Sketch illustrating the typical morphology of catchments experiencing an increase in uplift rate in the Apennines and the differences between catchments being uplifted at different rates (e.g., along-strike variations along a normal fault). (b) Schematic representation of typical river profile (blue) and sediment grain size (black) along a river in a footwall catchment responding to an increase in fault throw rate in the Apennines (catchment 2 in Figure 7a). Coarse sediment supply from landslides and scree cones downstream of main long-profile convexity leads to an increase in the grain size of the sediment in the river [*Whittaker et al.*, 2010].

nels. In addition, the prefactor k_w in equation (1) is inversely proportional to relative uplift rate in the studied catchments, with values of 2.1, 3.2, and 4.4 $m^{-1/8}$ $s^{3/8}$ obtained for fault throw rates after fault acceleration of 1.5 (Celano Gorge), 1.0 (Rio Torto), and 0.25 mm yr^{-1} (Torrente l'Apa), respectively. This latter observation is consistent with experimental work by *Turowski et al.* [2006]. Importantly, the Celano Gorge which is experiencing a relative uplift rate 50% higher than Rio Torto has a k_w coefficient 50% lower: most of the difference in relative uplift rate is here accommodated by channel narrowing, suggesting that channel width does not only depend on discharge and slope and that channel narrowing is enhanced at high relative uplift rate. Recent modeling studies of the evolution of the cross section

of a channel have challenged the validity of equation (1), and in particular the assumption that the width-to-depth ratio is constant (on which it is based). Field data in Italy and Taiwan supports the idea that width-to-depth ratio is variable in bedrock rivers [*Whittaker et al.*, 2007a; *Yanites and Tucker*, 2010]. *Turowski et al.*'s [2009] model including an erosion threshold showed that, for uplift rates increasing beyond a given value, channels narrow and channel width-to-depth ratio increases. *Yanites and Tucker* [2010] included the role that sediment plays in inhibiting bedrock erosion in their model. Their model predicts that the width-to-depth ratio is constant and that equation (1) adequately describes the dependency of channel width on discharge and slope at low sediment supply to transport capacity ratio. Conversely, for moderate to high sediment fluxes, channels narrow as slope increase, the width-to-depth ratio decreases with increasing uplift rate (as shown by the field data) and the trends observed are exacerbated by increasing sediment fluxes [*Yanites and Tucker*, 2010]. This demonstrates that, in addition to slope and discharge, sediment may play an essential role in controlling channel geometry in the Apennines, even if sediment fluxes through the studied catchments are relatively low compared to fluxes in regions like Taiwan or the Himalayas [*Yanites and Tucker*, 2010]. Thus, by including changes in channel geometry via the varying prefactor k_w, the role of sediment is indirectly incorporated in our approach.

4.1.4. Landscape Response Time and Threshold for Erosion

[32] Our results show that the higher the τ_c value, the larger the increase in the migration rate of long-profile convexity with increasing uplift rate (Figure 6). In addition, the retreat rate of the convexity generally increases with increasing τ_c for each catchment. This result is due to the way calibration is carried out (section 3.3). The steepened reach of the Rio Torto was used as a reference for calibration: when τ_c is raised, the erosive efficiency of the river is lowered so the erodibility coefficient k_b has to be increased to fit the steepened reach along the profile of Rio Torto. Two effects are competing here: the retreat rate of long-profile convexities should increase with increasing k_b [*Rosenbloom and Anderson*, 1994; *Attal et al.*, 2008] but it should decrease with increasing τ_c, because the time that the convexity spends actively retreating is reduced (no erosion happens during floods that generate stresses below the threshold). The fact that convexities propagate faster when τ_c is raised in all three catchments (Figure 6) suggests that the former effect (erodibility) is dominant in our experiments. The timing of the response to fault acceleration is good for Torrente l'Apa but convexities tend to propagate too quickly for Rio Torto and Celano Gorge, even with $\tau_c = 0$ (Figure 6): the best fit in terms of location of the main long-profile convexity is achieved too early after fault acceleration (Figure 5). Whereas one explanation is that the detachment-limited model is unable to fully capture the temporal evolution of the studied catchments, an alternative explanation involves the role of changing climate over the Quaternary. In our model, we assumed that climate is constant over the duration of the runs and we calibrated our climate parameters against modern climate data (section 3.1). However, the Quaternary is characterized by numerous climatic fluctuations between glacial and interglacial conditions that have affected the study area [*Tzedakis*, 2005]. If the current conditions and the climate parameters chosen underestimate the global erosive efficiency of the rivers over the duration of the runs, then the erodibility coefficient may have been overestimated, with potential impact on the predicted retreat rate of long-profile convexities. However, in our model where thresholds for erosion, a slope-dependent channel width and an uplift-dependent k_w coefficient introduce a strong nonlinear component in the relationship between stream power and erosion rates, the influence of changing climate during the runs on the predicted response of the landscape is not easy to forecast and is beyond the scope of this study.

4.1.5. Deviations Between Modeled and Real Profiles

[33] Whereas the detachment-limited model can explain the overall steepening of the river profiles and the location of the main long-profile convexities in response to an increase in relative uplift rate, it fails to replicate the detailed response of the landscape: the model predicts an approximately constant slope along the steepened reaches of the three catchments (Figure 5), the monotonic downstream increase in uplift rate being largely counterbalanced by the increase in drainage area. Such prediction is consistent with the shape of the Rio Torto profile but does not satisfyingly account for local variations in slope along the profiles of Torrente l'Apa and Celano Gorge. These local variations will cause large fluctuations in specific stream power or shear stress which will not be related to variations in uplift rate. Despite including the role of thresholds for erosion and a slope-dependent channel width, our model is too simplistic in that it does not account for local controls on stream power and erosion rates. These local controls may include the role of stochastic sediment supply to the channel [e.g., *Benda and Dunne*, 1997], in particular since numerous landslides have been largely documented along the steepened reaches of the studied catchments (Figures 1b–1d). A landslide may inhibit erosion locally by burying the bedrock under a protective cover that may take decades to millennia to be removed [e.g., *Lague*, 2010; *Yanites et al.*, 2010b]. On the other hand, within the framework of *Turowski et al.*'s [2007] model of bedrock erosion, such a pulse of sediment to one of the studied rivers which are typically starved of sediment should enhance fluvial incision downstream by providing tools for bedrock erosion [*Turowski et al.*, 2007]. This situation (inhibition of erosion locally and promotion of erosion downstream) should generate local slope changes and may thus explain some details of the shape of Torrente l'Apa and Celano Gorge's river profiles, particularly the relatively low slopes immediately upstream of the fault (Figure 5). Further testing of fluvial incision laws using sediment-flux-dependent models will be required to assess whether including the potential role of sediment particles as tools and/or cover with respect to bedrock erosion [e.g., *Gilbert*, 1877; *Sklar and Dietrich*, 1998, 2001, 2004; *Turowski et al.*, 2007] would lead to greater capacity to predict the response and geometry of catchments perturbed by tectonics, and whether the observed local slope variations are important for understanding the overall landscape response of tectonically perturbed catchments.

4.2. Implications for Modeling Landscape Evolution and Extracting Tectonic Signals From Topography

4.2.1. Field Observations and Model Comparison

[34] Based on the response of three catchments of different sizes which have been perturbed tectonically to various extents, this work suggests that the detachment-limited model, with the addition of an appropriate threshold and a slope-dependent channel width, adequately describes the overall shape of the studied landscape. *Lavé and Avouac* [2001] came to a similar conclusion with their study of rivers at the active front of the Himalayas. Based on the analysis of landscapes in Northern and Southern California, *Snyder et al.*'s [2003a, 2003b] and *DiBiase et al.*'s [2010] studies, respectively, also gave some support to the detachment-limited model including a threshold for erosion.

[35] Clearly, our results and conclusions differ markedly from those of *Loget et al.* [2006] and *Valla et al.* [2010], where the transient response was found to be diffusive and quite well described by a transport-limited model, in contrast to the wave-like response of a detachment-limited system that we observe. Both *Loget et al.* [2006] and *Valla et al.* [2010] document bedrock incision for rivers where the change in base level is sudden and not sustained (as a result of lowering of the Mediterranean sea level during the Messinian salinity crisis and deglaciation, respectively), causing large convexities and substantial steepened reaches to appear almost instantly (geologically speaking) in the lower part of the river profiles. Such situation seems to promote a progressive degradation of the main profile convexity that the detachment-limited model is unable to account for. The mechanisms responsible for this behavior in this particular setting are unknown but probably involve feedbacks between gorge formation along the steep reaches, sediment supply into the gorge from steep hillslopes and the necessity for the river to mobilize significant amounts of sediment during floods to erode its bedrock [*Valla et al.*, 2010]. Furthermore, a diffuse transient response to fault acceleration has been documented in a catchment draining across an active fault in Greece, even though the tectonic history and bedrock geology of this catchment is very similar to that of the present study [*Cowie et al.*, 2008]. The main difference between the Greek example and the studied rivers in the Italian Apennines is that the limestone which is actively incised by the Xerias River in Greece is shrouded by a layer of Plio-Pleistocene fluvial conglomerates which are poorly consolidated [*Cowie et al.*, 2008]. These conglomerates supply perfectly rounded and potentially mobile pebbles (with diameter rarely exceeding 100 mm) which are actively transported all along the river, leading to very poor bedrock exposure (the bed is typically blanketed with sediment and bed exposure never exceeds 20%). The presence of a quasi-continuous sediment cover in the Xerias River and the absence of long-profile convexities upstream of the active fault along the actively incising river suggest that sediment transport is the main control on the gradient of the river, thus leading to a diffuse response to an increase in fault throw rate. Specifically, moving sediment during floods leads to changes in the degree of bed cover which thus modulates bedrock erosion, allowing the river to keep pace with the uplift rate at the fault.

4.2.2. Selecting Landscape Evolution Models

[36] Based on our results and discussion (section 4.2.1), we suggest that basic field observations and measurements can help constrain the models that should be used to simulate the landscape evolution of a given area or to map spatial variations in fluvial erosion rates (Table 2). The scarcity or absence of bed exposure along a river seems to preclude the use of the detachment-limited model, even if the river is actively incising into bedrock [*Cowie et al.*, 2008]. In the presence of moderate or low amounts of sediment however, using a detachment-limited model including a threshold for erosion would be appropriate: this model explains best the evolution of the studied catchments (Table 2 and see section 4.2.2) and patterns of fluvial erosion at the front of the Himalayas [*Lavé and Avouac*, 2001] and across mountain ranges in California [*Snyder et al.*, 2003a, 2003b; *DiBiase et al.*, 2010]. *Snyder et al.* [2003a, 2003b] and *DiBiase et al.* [2010] showed that typical hydraulic scaling relationships can account for the evolution of channel width through catchments in quasi-equilibrium experiencing quasi-uniform uplift. However, if the response of the landscape to a perturbation is to be predicted and/or if the uplift field across the studied catchment is nonuniform [*Lavé and Avouac*, 2001], we suggest that a slope-dependent channel width should be included in the model, e.g., using equation (1). Even if such an equation does not incorporate the additional potential controls on channel width (e.g., role of sediment), it accounts for the now widely documented phenomenon that channel slope cannot adjust without changing the width and vice versa [*Stark*, 2006; *Wobus et al.*, 2006b; *Turowski et al.*, 2007, 2009; *Yanites and Tucker*, 2010]. Ideally, the threshold value τ_c as well as the prefactor k_w in equation (1) would be calibrated against field data (Table 2). The threshold value should be calculated using the median grain size of the fluvial sediment D_{50} [*Lavé and Avouac*, 2001; this study]. We highlight that variations in the grain size of the sediment along the river would lead to changes in the threshold value (see section 4.1.2 and Figure 7) and that further work is needed to constrain spatial and temporal variations in sediment caliber (and thus erosion threshold) induced by changes in hillslope erosion rates and processes as landscapes respond to changes in boundary conditions (tectonics, climate) [e.g., *Whittaker et al.*, 2010].

4.2.3. Tectonics From Topography?

[37] Steepness indices are commonly used in the literature to assess tectonics from topography using remotely sensed data [e.g., *Kirby et al.*, 2003; *Wobus et al.*, 2006a; *Miller et al.*, 2007]. They are usually calculated using a reference concavity index of 0.45–0.5 which is the typical concavity of steady state channels in uniformly uplifted landscapes (for methods, see *Wobus et al.* [2006a]); differences in steepness index along a river or between adjacent rivers thus represent deviations from the typical steady state profile and could be interpreted in terms of spatially variable uplift or transient response of the landscape to a perturbation. However, care must be taken when interpreting such data because changes in channel width and the existence of a threshold for erosion can also affect the steepness of rivers by modulating their erosive efficiency [*Snyder et al.*, 2003b; *Whittaker et al.*, 2008]. We believe that maps showing

Table 2. Recommendations for Modeling Landscape Evolution or Estimating the Distribution of Fluvial Erosion Rates Across a Landscape, Based on Our Results

Field Observations	Modeling Landscape Evolution	Mapping the Distribution of Fluvial Erosion Rates
Amount of sediment in river		
Low–moderate	Detachment-limited model with threshold suitable to model landscape evolution. Ideally, τ_c should be calibrated against field-derived D_{50} value (spatially variable?).	Maps of SSP or shear stress in excess of threshold may provide a better representation of the distribution of fluvial erosion rates than maps of steepness index. Ideally, τ_c should be calibrated against field-derived D_{50} value (spatially variable?).
High	Detachment-limited model not suitable to model landscape evolution.	Steepness index, SSP, or shear stress maps may provide an inaccurate representation of the distribution of fluvial erosion rates.
Channel width		
Obeys typical hydraulic scaling [*Leopold and Maddock*, 1953]	Use equation $W = k_w Q^{1/2}$ in the model, with k_w calibrated against data from real landscape (field or DEM derived).	Use equation $W = k_w Q^{1/2}$ to calculate W to be used in SSP or shear stress equations.
Shows slope dependency	Use equation $W = k_w Q^{3/8} S^{-3/16}$ in the model, with k_w calibrated against data from real landscape (field or DEM derived).	Use equation $W = k_w Q^{3/8} S^{-3/16}$ to calculate W to be used in SSP or shear stress equations.
Shows no predictable trend	No suitable model to simulate landscape evolution.	Use punctual width measurements (field or DEM derived) to calculate SSP or shear stress at various points along the river.

specific stream power or shear stress in excess of the threshold for erosion [*Snyder et al.*, 2003a, 2003b; *Lague et al.*, 2005] that also account for potential channel width adjustment [*Finnegan et al.*, 2005; *Stark*, 2006; *Wobus et al.*, 2006b; *Turowski et al.*, 2007; *Whittaker et al.*, 2007a; *Yanites et al.*, 2010a] would give a more accurate representation of variations in fluvial erosion rates – and thus potential variations in uplift rates – across landscapes than maps of steepness indices (Table 2). Ideally, thresholds for erosion would be calibrated against field data (using fluvial sediment D_{50}), while using channel width values measured in the field or extracted from a DEM (if its resolution is good enough) would yield more accurate values of specific stream power or shear stress, whether channels are adjusting or not.

4.2.4. Limitations

[38] We emphasize that the detachment-limited model would not be suitable for modeling the evolution of landscapes dissected by rivers transporting large amounts of sediment (sections 4.2.1 and 4.2.2). Similarly, maps of specific stream power or shear stress along such rivers would provide a poor picture of the distribution of erosion rates along the rivers (Table 2). Care must therefore be taken when using such approaches to compute numerically the evolution of a landscape or to estimate relative fluvial erosion rates in an area, as a river which transports relatively low amounts of sediment at the present-day may have been choked with sediment in the past, possibly because of changes in the type of supply from hillslopes: for example, the characteristics of glacially derived sediment differ from those of hillslope-derived sediment [e.g., *Attal and Lavé*, 2006]; a change in the lithology exposed in the catchment (e.g., through the exhumation of different rock types) may alter the bed load to total load ratio, because of a different ratio at the source and/or different abrasion rates [*Attal and Lavé*, 2006, 2009]; climate change can alter vegetation and runoff on the hillslopes and may potentially lead to large alluviation events in mountain rivers [e.g., *Pratt-Sitaula et al.*, 2004]. In addition to temporal changes in sediment fluxes, the model outcomes will also be affected by spatial variations in sediment fluxes, in particular at the downstream transition from detachment-limited to transport-limited behavior which has been documented along the course of incising rivers, in theory [*Whipple and Tucker*, 2002] and in the field [*Brocard and van der Beek*, 2006].

[39] Sediment fluxes which are ignored in the approaches described in this paper may also be responsible for changes in channel geometry that the equation used to calculate channel width (equation (1)) fails to predict. Our data clearly shows that channel width in the studied area is not dependent solely on discharge and slope and that channel is enhanced as uplift rate increases, an effect that we replicated by adjusting the prefactor k_w in equation (1) (section 4.1.3). *Yanites and Tucker*'s [2010] model demonstrates that despite sediment fluxes being relatively low in the studied catchments, they may be responsible for this enhanced narrowing and for the changes in width-to-depth ratio which have been documented in the field-derived data [*Whittaker et al.*, 2007a; *Yanites and Tucker*, 2010].

[40] Finally, whereas the detachment-limited model with threshold for erosion and a slope-dependent channel width reproduces the overall shape of the studied catchments in the Apennines, it fails to account for local variations in slope that cause fluctuation in specific stream power which are not related to changes in uplift rates (see section 4.1.5 and Figure 5). We thus emphasize that the predictions of the model, in terms of landscape evolution or quantification of fluvial erosion rates in a given area, are valid on the large scale (i.e., at suprakilometric scale), and that local deviations from the general trend in the data derived from the real landscape (e.g., real river profile, maps of fluvial incision rates) may result from processes which affect fluvial incision rates locally and that the model does not account for, such as stochastic sediment supply from the hillslopes [e.g., *Benda and Dunne*, 1997; *Yanites et al.*, 2010b]. Further

studies are required to better understand the links between climate, tectonics, sediment generation on the hillslopes, sediment supply to river, channel geometry adjustment, fluvial sediment transport and bedrock erosion, and thus design and test better fluvial erosion models that will make accurate predictions of fluvial erosion rates and landscape evolution at all scales, from river reaches to mountain ranges.

5. Conclusion

[41] This test of fluvial erosion models using three transient catchments in the Apennines favors a detachment-limited model with a threshold for erosion and a slope-dependent channel width. Unlike the transport-limited model and the basic detachment-limited model (no threshold for erosion, channel width is a simple function of drainage area), this model reproduces the overall shape of the river profiles as well as both the location and height of the main long-profile convexity that formed in response to an independently constrained increase in relative uplift rate ~0.75 Ma ago. The hydraulic scaling equation proposed by *Finnegan et al.* [2005] (equation (1)) which includes a slope dependency to express channel width was used in this study. The prefactor k_w in equation (1) calibrated against field data is strongly dependent on relative uplift rate, showing that equation (1) tends to underestimate the amount of narrowing that a river can undergo as it steepens. Our results show that changes in channel geometry exert an important control on landscape response time: the dependency of channel width on slope and the uplift-dependent prefactor k_w are responsible for a substantial increase in the migration rate of long-profile convexities with increasing uplift rate (Figure 6), which has been observed in the study area [*Whittaker et al.*, 2008]. A threshold of 38 Pa corresponding to the shear stress required to move sediments with a grain size of 50 mm, similar to the median grain size of the fluvial sediment along the steepened reaches in the study area, is required to fit the location and height of the main long-profile convexities in the three catchments. The modeled response times vary (0.35–0.75Ma) for a threshold of 38 Pa (Figure 5), and are somewhat younger that the field observations indicate (~0.75 Ma), but are broadly consistent given the uncertainties in long-term climatic controls that we are not able to include in our approach.

[42] Based on these results, we suggest that maps of specific shear stress or stream power in excess of an erosion threshold that also account for dynamic channel adjustment would bring more precise information on the spatial distribution of fluvial erosion rates than maps of steepness indices which rely solely on slope and drainage area to highlight the deviations from the typical steady state concave up profile of rivers incising into uniformly uplifted landscapes. Additionally, we suggest that basic field observations and measurements of channel geometry and sediment characteristics can help choose and calibrate the best fluvial erosion model to predict the evolution of a given landscape (Table 2). Grain size data can be used to calibrate the threshold for a detachment-limited model to predict the evolution of a landscape incised by rivers transporting low to moderate amounts of sediments. In all cases, a slope-dependent channel width should be included in the model to account for the now widely accepted fact that channels narrow as they steepen [e.g., *Yanites and Tucker*, 2010]. Our results demonstrate that simple detachment-limited models are suitable to reproduce the evolution of catchments, such as those in the Apennines, with a reasonable degree of fidelity. However, assessing the extent to which local sediment supply variations need to be included in the models in order to make high-resolution predictions of landscape evolution remains an outstanding challenge for the future.

[43] **Acknowledgments.** This project was funded by the NERC Research grants NE/B504165/1 (Cowie, Roberts, Attal, and Tucker), NER/S/A/2002/10359 (Whittaker), and GR9/02995 (Roberts, Michetti) and by NSF and ARO (EAR-0643240 and 47033-EV; Tucker). We are grateful to Nicole Gasparini, Jens Turowski, and the editor and associate editor for detailed comments and suggestions which notably improved this manuscript. We thank Eutizio Vittorio (APAT) for the DEM from which we derived the triangulated irregular network used in the numerical model.

References

Amos, C. B., and D. W. Burbank (2007), Channel width response to differential uplift, *J. Geophys. Res.*, *112*, F02010, doi:10.1029/2006JF000672.

Anders, M. H., M. Spiegelman, D. W. Rodgers, and J. T. Hagstrum (1993), The growth of fault-bounded tilt blocks, *Tectonics*, *12*, 1451–1459, doi:10.1029/93TC01547.

Attal, M., and J. Lavé (2006), Changes of bedload characteristics along the Marsyandi River (central Nepal): Implications for understanding hillslope sediment supply, sediment load evolution along fluvial networks, and denudation in active orogenic belts, *Spec. Pap. Geol. Soc. Am.*, *398*, 143–171, doi:10.1130/2006.2398(09).

Attal, M., and J. Lavé (2009), Pebble abrasion during fluvial transport: Experimental results and implications for the evolution of the sediment load along rivers, *J. Geophys. Res.*, *114*, F04023, doi:10.1029/2009JF001328.

Attal, M., G. E. Tucker, A. C. Whittaker, P. A. Cowie, and G. P. Roberts (2008), Modeling fluvial incision and transient landscape evolution: Influence of dynamic channel adjustment, *J. Geophys. Res.*, *113*, F03013, doi:10.1029/2007JF000893.

Benda, L., and T. Dunne (1997), Stochastic forcing of sediment supply to channel networks from landsliding and debris flow, *Water Resour. Res.*, *33*, 2849–2863, doi:10.1029/97WR02388.

Boulton, S. J., and A. C. Whittaker (2009), Quantifying the slip rates, spatial distribution and evolution of active normal faults from geomorphic analysis: Field examples from an oblique-extensional graben, southern Turkey, *Geomorphology*, *104*, 299–316, doi:10.1016/j.geomorph.2008.09.007.

Brocard, G. Y., and P. A. van der Beek (2006), Influence of incision rate, rock strength, and bedload supply on bedrock river gradients and valley-flat widths: Field based evidence and calibrations from western Alpine rivers (southeast France), *Spec. Pap. Geol. Soc. Am.*, *398*, 101–126.

Buffington, J. M., and D. R. Montgomery (1997), A systematic analysis of eight decades of incipient motion studies, with special reference to gravel-bedded rivers, *Water Resour. Res.*, *33*, 1993–2029, doi:10.1029/96WR03190.

Burbank, D. W., J. Leland, E. Fielding, R. S. Anderson, N. Brozovic, M. R. Reid, and C. Duncan (1996), Bedrock incision, rock uplift and threshold hillslopes in the northwestern Himalayas, *Nature*, *379*, 505–510, doi:10.1038/379505a0.

Chatanantavet, P., and G. Parker (2009), Physically based modeling of bedrock incision by abrasion, plucking, and macroabrasion, *J. Geophys. Res.*, *114*, F04018, doi:10.1029/2008JF001044.

Cowie, P. A., A. C. Whittaker, M. Attal, G. P. Roberts, G. E. Tucker, and A. Ganas (2008), New constraints on sediment-flux-dependent river incision: Implications for extracting tectonic signals from river profiles, *Geology*, *36*, 535–538, doi:10.1130/G24681A.1.

Crosby, B. T., and K. X. Whipple (2006), Knickpoint initiation and distribution within fluvial networks: 236 waterfalls in the Waipaoa River, North Island, New Zealand, *Geomorphology*, *82*, 16–38, doi:10.1016/j.geomorph.2005.08.023.

DiBiase, R. A., K. X. Whipple, A. M. Heimsath, and W. B. Ouimet (2010), Landscape form and millennial erosion rates in the San Gabriel Mountains, CA, *Earth Planet. Sci. Lett.*, *289*, 134–144, doi:10.1016/j.epsl.2009.10.036.

Eagleson, P. S. (1978), Climate, soil, and vegetation: 2. Distribution of annual precipitation derived from observed storm sequences, *Water Resour. Res.*, *14*, 713–721, doi:10.1029/WR014i005p00713.

Ellis, M. A., A. L. Densmore, and R. S. Anderson (1999), Development of mountainous topography in the Basin Ranges, USA, *Basin Res.*, *11*, 21–41, doi:10.1046/j.1365-2117.1999.00087.x.

Finnegan, N. J., G. Roe, D. R. Montgomery, and B. Hallet (2005), Controls on the channel width of rivers: Implications for modeling fluvial incision of bedrock, *Geology*, *33*, 229–232, doi:10.1130/G21171.1.

Gasparini, N. M., R. L. Bras, and K. X. Whipple (2006), Numerical modeling of non-steady state river profile evolution using a sediment-flux-dependent incision model, *Spec. Pap. Geol. Soc. Am.*, *398*, 127–141.

Gasparini, N. M., K. X. Whipple, and R. L. Bras (2007), Predictions of steady state and transient landscape morphology using sediment-flux-dependent river incision models, *J. Geophys. Res.*, *112*, F03S09, doi:10.1029/2006JF000567.

Gilbert, G. K. (1877), Report on the geology of the Henry Mountains: Geographical and geological survey of the rocky mountain region, report, 160 pp., Dep. of the Inter., Washington D. C.

Hawk, K. L. (1992), Climatology of station storm rainfall in the continental United States: Parameters of the Bartlett-Lewis and Poisson rectangular pulses models, M.S. thesis, Mass. Inst. of Tech., Cambridge, Mass.

Howard, A. D. (1994), A detachment-limited model of drainage-basin evolution, *Water Resour. Res.*, *30*, 2261–2285, doi:10.1029/94WR00757.

Howard, A. D., and G. Kerby (1983), Channel changes in badlands, *Geol. Soc. Am. Bull.*, *94*, 739–752, doi:10.1130/0016-7606(1983)94<739:CCIB>2.0.CO;2.

Howard, A. D., W. E. Dietrich, and M. A. Seidl (1994), Modeling fluvial erosion on regional to continental scales, *J. Geophys. Res.*, *99*, 13,971–13,986, doi:10.1029/94JB00744.

Johnson, J. P. L., K. X. Whipple, L. S. Sklar, and T. C. Hanks (2009), Transport slopes, sediment cover, and bedrock channel incision in the Henry Mountains, Utah, *J. Geophys. Res.*, *114*, F02014, doi:10.1029/2007JF000862.

Kirby, E., and K. Whipple (2001), Quantifying differential rock-uplift rates via stream profile analysis, *Geology*, *29*, 415–418, doi:10.1130/0091-7613(2001)029<0415:QDRURV>2.0.CO;2.

Kirby, E., K. X. Whipple, W. Q. Tang, and Z. L. Chen (2003), Distribution of active rock uplift along the eastern margin of the Tibetan Plateau: Inferences from bedrock channel longitudinal profiles, *J. Geophys. Res.*, *108*(B4), 2217, doi:10.1029/2001JB000861.

Kooi, H., and C. Beaumont (1994), Escarpment evolution on high-elevation rifted margins: Insights derived from a surface processes model that combines diffusion, advection, and reaction, *J. Geophys. Res.*, *99*, 12,191–12,209, doi:10.1029/94JB00047.

Lague, D. (2010), Reduction of long-term bedrock incision efficiency by short-term alluvial cover intermittency, *J. Geophys. Res.*, *115*, F02011, doi:10.1029/2008JF001210.

Lague, D., N. Hovius, and P. Davy (2005), Discharge, discharge variability, and the bedrock channel profile, *J. Geophys. Res.*, *110*, F04006, doi:10.1029/2004JF000259.

Lavé, J., and J. P. Avouac (2001), Fluvial incision and tectonic uplift across the Himalayas of central Nepal, *J. Geophys. Res.*, *106*, 26,561–26,591, doi:10.1029/2001JB000359.

Lavé, J., and D. Burbank (2004), Denudation processes and rates in the Transverse Ranges, Southern California: Erosional response of a transitional landscape to external and anthropogenic forcing, *J. Geophys. Res.*, *109*, F01006, doi:10.1029/2003JF000023.

Leopold, L. B., and T. Maddock (1953), The hydraulic geometry of stream channels and some physiographic implications, *U.S. Geol. Surv. Prof. Pap.*, *252*, 57 pp.

Loget, N., P. Davy, and J. Van Den Driessche (2006), Mesoscale fluvial erosion parameters deduced from modeling the Mediterranean sea level drop during the Messinian (late Miocene), *J. Geophys. Res.*, *111*, F03005, doi:10.1029/2005JF000387.

Meyer-Peter, E., and R. Müller (1948), Formulas for bed-load transport, in *Proceedings of the 2nd Meeting of the International Association for Hydraulic Structures Research*, pp. 39–64, Int. Assoc. Hydraul. Res., Delft, Netherlands.

Miller, S. R., R. L. Slingerland, and E. Kirby (2007), Characteristics of steady state fluvial topography above fault-bend folds, *J. Geophys. Res.*, *112*, F04004, doi:10.1029/2007JF000772.

Pratt-Sitaula, B., D. W. Burbank, A. Heimsath, and T. Ojha (2004), Landscape disequilibrium on 1000–10,000 year scales, Marsyandi River, Nepal, central Himalaya, *Geomorphology*, *58*, 223–241, doi:10.1016/j.geomorph.2003.07.002.

Rickenmann, D., (2001), Comparison of bed load transport in torrents and gravel bed streams, *Water Resour. Res.*, *37*, 3295–3305, doi:10.1029/2001WR000319.

Roberts, G. P., and A. M. Michetti (2004), Spatial and temporal variations in growth rates along active normal fault systems: An example from The Lazio-Abruzzo Apennines, central Italy, *J. Struct. Geol.*, *26*, 339–376, doi:10.1016/S0191-8141(03)00103-2.

Roering, J. J., J. W. Kirchner, and W. E. Dietrich (1999), Evidence for nonlinear, diffusive sediment transport on hillslopes and implications for landscape morphology, *Water Resour. Res.*, *35*, 853–870, doi:10.1029/1998WR900090.

Rosenbloom, N. A., and R. S. Anderson (1994), Hillslope and channel evolution in a marine terraced landscape, Santa Cruz, California, *J. Geophys. Res.*, *99*, 14,013–14,029, doi:10.1029/94JB00048.

Seidl, M. A., and W. E. Dietrich (1992), The problem of channel erosion into bedrock, *Catena*, *23*, suppl., 101–124.

Sklar, L. S., and W. E. Dietrich (1998), River longitudinal profiles and bedrock incision models: Stream power and the influence of sediment supply, in *Rivers Over Rock: Fluvial Processes in Bedrock Channels*, *Geophys. Monogr. Ser.*, vol. 107, edited by K. Tinkler and E. E. Wohl, pp. 237–260, AGU, Washington, D. C.

Sklar, L. S., and W. E. Dietrich (2001), Sediment and rock strength controls on river incision into bedrock, *Geol. Soc. Am. Bull.*, *29*, 1087–1090.

Sklar, L. S., and W. E. Dietrich (2004), A mechanistic model for river incision into bedrock by saltating bed load, *Water Resour. Res.*, *40*, W06301, doi:10.1029/2003WR002496.

Sklar, L. S., and W. E. Dietrich (2006), The role of sediment in controlling steady state bedrock channel slope: Implications of the saltation–abrasion incision model, *Geomorphology*, *82*, 58–83, doi:10.1016/j.geomorph.2005.08.019.

Sklar, L. S., W. E. Dietrich, E. Foufoula-Georgiou, B. Lashermes, and D. Bellugi (2006), Do gravel bed river size distributions record channel network structure?, *Water Resour. Res.*, *42*, W06D18, doi:10.1029/2006WR005035.

Snyder, N. P., and L. L. Kammer (2008), Dynamic adjustments in channel width in response to a forced diversion: Gower Gulch, Death Valley National Park, *Calif. Geol.*, *36*, 187–190.

Snyder, N. P., K. X. Whipple, G. E. Tucker, and D. J. Merritts (2003a), Channel response to tectonic forcing: Field analysis of stream morphology and hydrology in the Mendocino triple junction region, northern California, *Geomorphology*, *53*, 97–127, doi:10.1016/S0169-555X(02)00349-5.

Snyder, N. P., K. X. Whipple, G. E. Tucker, and D. J. Merritts (2003b), Importance of a stochastic distribution of floods and erosion thresholds in the bedrock river incision problem, *J. Geophys. Res.*, *108*(B2), 2117, doi:10.1029/2001JB001655.

Stark, C. P. (2006), A self-regulating model of bedrock river channel geometry, *Geophys. Res. Lett.*, *33*, L04402, doi:10.1029/2005GL023193.

Stock, J. D., and D. R. Montgomery (1999), Geologic constraints on bedrock river incision using the stream power law, *J. Geophys. Res.*, *104*, 4983–4993, doi:10.1029/98JB02139.

Tomkin, J. H., M. T. Brandon, F. J. Pazzaglia, J. R. Barbour, and S. D. Willett (2003), Quantitative testing of bedrock incision models for the Clearwater River, NW Washington state, *J. Geophys. Res.*, *108*(B6), 2308, doi:10.1029/2001JB000862.

Tucker, G. E. (2004), Drainage basin sensitivity to tectonic and climatic forcing: Implications of a stochastic model for the role of entrainment and erosion thresholds, *Earth Surf. Processes Landforms*, *29*, 185–205, doi:10.1002/esp.1020.

Tucker, G. E., and R. L. Bras (2000), A stochastic approach to modeling the role of rainfall variability in drainage basin evolution, *Water Resour. Res.*, *36*, 1953–1964, doi:10.1029/2000WR900065.

Tucker, G. E., and K. X. Whipple (2002), Topographic outcomes predicted by stream erosion models: Sensitivity analysis and intermodel comparison, *J. Geophys. Res.*, *107*(B9), 2179, doi:10.1029/2001JB000162.

Tucker, G. E., S. T. Lancaster, N. M. Gasparini, R. L. Bras, and S. M. Rybarczyk (2001), An object-oriented framework for distributed hydrologic and geomorphic modeling using triangulated irregular networks, *Comput. Geosci.*, *27*, 959–973, doi:10.1016/S0098-3004(00)00134-5.

Turowski, J. M., D. Lague, A. Crave, and N. Hovius (2006), Experimental channel response to tectonic uplift, *J. Geophys. Res.*, *111*, F03008, doi:10.1029/2005JF000306.

Turowski, J. M., D. Lague, and N. Hovius (2007), Cover effect in bedrock abrasion: A new derivation and its implications for the modeling of bedrock channel morphology, *J. Geophys. Res.*, *112*, F04006, doi:10.1029/2006JF000697.

Turowski, J. M., D. Lague, and N. Hovius (2009), Response of bedrock channel width to tectonic forcing: Insights from a numerical model, theoretical considerations, and comparison with field data, *J. Geophys. Res.*, *114*, F03016, doi:10.1029/2008JF001133.

Tzedakis, P. (2005), Towards an understanding of the response of southern European vegetation to orbital and suborbital climate variability, *Quat. Sci. Rev.*, *24*, 1585–1599, doi:10.1016/j.quascirev.2004.11.012.

Valla, P. G., P. A. van der Beek, and D. Lague (2010), Fluvial incision into bedrock: Insights from morphometric analysis and numerical modeling

of gorges incising glacial hanging valleys (Western Alps, France), *J. Geophys. Res.*, *115*, F02010, doi:10.1029/2008JF001079.

van der Beek, P., and P. Bishop (2003), Cenozoic river profile development in the Upper Lachlan catchment (SE Australia) as a test of quantitative fluvial incision models, *J. Geophys. Res.*, *108*(B6), 2309, doi:10.1029/2002JB002125.

Whipple, K. X., and G. E. Tucker (1999), Dynamics of the stream-power river incision model: Implications for height limits of mountain ranges, landscape response timescales, and research needs, *J. Geophys. Res.*, *104*, 17,661–17,674, doi:10.1029/1999JB900120.

Whipple, K. X., and G. E. Tucker (2002), Implications of sediment-flux-dependent river incision models for landscape evolution, *J. Geophys. Res.*, *107*(B2), 2039, doi:10.1029/2000JB000044.

Whipple, K. X., N. P. Snyder, and K. Dollenmayer (2000a), Rates and processes of bedrock incision by the upper Ukak River since the 1912 Novarupta ash flow in the Valley of Ten Thousand Smokes, Alaska, *Geology*, *28*, 835–838, doi:10.1130/0091-7613(2000)28<835:RAPOBI>2.0.CO;2.

Whipple, K. X., G. S. Hancock, and R. S. Anderson (2000b), River incision into bedrock: Mechanics and relative efficacy of plucking, abrasion and cavitation, *Geol. Soc. Am. Bull.*, *112*, 490–503, doi:10.1130/0016-7606(2000)112<490:RIIBMA>2.0.CO;2.

Whittaker, A. C., P. A. Cowie, M. Attal, G. E. Tucker, and G. P. Roberts (2007a), Bedrock channel adjustment to tectonic forcing: Implications for predicting river incision rates, *Geology*, *35*, 103–106, doi:10.1130/G23106A.1.

Whittaker, A. C., P. A. Cowie, M. Attal, G. E. Tucker, and G. P. Roberts (2007b), Contrasting transient and steady state rivers crossing active normal faults: New field observations from the central Apennines, Italy, *Basin Res.*, *19*, 529–556, doi:10.1111/j.1365-2117.2007.00337.x.

Whittaker, A. C., M. Attal, P. A. Cowie, G. E. Tucker, and G. P. Roberts (2008), Decoding temporal and spatial patterns of fault uplift using transient river long profiles, *Geomorphology*, *100*, 506–526, doi:10.1016/j.geomorph.2008.01.018.

Whittaker, A. C., M. Attal, and P. A. Allen (2010), Characterising the origin, nature and fate of sediment exported from catchments perturbed by active tectonics, *Basin Res.*, *22*, 809–828, doi:10.1111/j.1365-2117.2009.00447.x.

Willgoose, G., R. L. Bras, and J. Rodriguez-Iturbe (1991), A coupled channel network growth and hillslope evolution model: 1. Theory, *Water Resour. Res.*, *27*, 1671–1684, doi:10.1029/91WR00935.

Wobus, C., K. X. Whipple, E. Kirby, N. Snyder, J. Johnson, K. Spyropolou, B. Crosby, and D. Sheehan (2006a), Tectonics from topography: Procedures, promise, and pitfalls, *Spec. Pap. Geol. Soc. Am.*, *398*, 55–74.

Wobus, C. W., G. E. Tucker, and R. S. Anderson (2006b), Self-formed bedrock channels, *Geophys. Res. Lett.*, *33*, L18408, doi:10.1029/2006GL027182.

Wobus, C. W., B. T. Crosby, and K. X. Whipple (2006c), Hanging valleys in fluvial systems: Controls on occurrence and implications for landscape evolution, *J. Geophys. Res.*, *111*, F02017, doi:10.1029/2005JF000406.

Yager, E. M., J. W. Kirchner, and W. E. Dietrich (2007), Calculating bed load transport in steep boulder bed channels, *Water Resour. Res.*, *43*, W07418, doi:10.1029/2006WR005432.

Yanites, B. J., and G. E. Tucker (2010), Controls and limits on bedrock channel geometry, *J. Geophys. Res.*, *115*, F04019, doi:10.1029/2009JF001601.

Yanites, B. J., G. E. Tucker, K. J. Mueller, Y.-G. Chen, T. Wilcox, and S. Y. Huang (2010a), Incision and channel morphology across active structures in the Peikang River, central Taiwan: Implications for the importance of channel width, *Geol. Soc. Am. Bull.*, *122*, 1192–1208, doi:10.1130/B30035.1.

Yanites, B. J., G. E. Tucker, K. J. Mueller, and Y.-G. Chen (2010b), How rivers react to large earthquakes: Evidence from central Taiwan, *Geology*, *38*, 639–642, doi:10.1130/G30883.1.

M. Attal, P. A. Cowie, and D. Hobley, School of GeoSciences, University of Edinburgh, Drummond Street, Edinburgh EH8 9XP, UK. (mikael.attal@ed.ac.uk)

G. P. Roberts, Research School of Geological and Geophysical Sciences, Birkbeck, University of London, and University College London, Gower Street, London WC1E 6BT, UK.

G. E. Tucker, Cooperative Institute for Research in Environmental Sciences, University of Colorado at Boulder, Boulder, CO 80309, USA.

A. C. Whittaker, Royal School of Mines, Imperial College London, South Kensington Campus, London SW7 2AZ, UK.